Polymer Testing 113 (2022) 107665

Contents lists available at ScienceDirect

Polymer Testing

journal homepage: www.elsevier.com/locate/polytest

Tensile behavior analysis combined with digital image correlation and mechanical and thermal properties of microfibrillated cellulose fiber/polylactic acid composites

Luiz C.C. Jesus [a], Janaíne M. Oliveira [b], Rosineide M. Leão [c], Lílian R. Beltrami [d], Ademir J. Zattera [d], Carla T.M. Anflor [e], Thiago C.R. Doca [a], Sandra M. Luz [a,e,*]

[a] Mechanical Sciences Program, Mechanical Engineering, University of Brasília, Brasília, DF, Brazil
[b] Civil Engineering Department, Ceres Campus, Unievangelica Centro Universitário, Ceres, GO, Brazil
[c] Institute of Exact Sciences and Technology, Paulista University, Brasília, DF, Brazil
[d] Process and Technology Engineering Program, University of Caxias do Sul, Caxias do Sul, RS, Brazil
[e] Automotive Engineering, Gama Campus, University of Brasília, Brasília, DF, Brazil

ARTICLE INFO

Keywords:
Microfibrillated cellulose
Curaua fibers
Polylactic acid
Composites
Digital image correlation

ABSTRACT

Microfibrillated cellulose (MFC) employed as reinforcement of polymeric matrices can increase elastic modulus, stiffness and strength of a composite. In this work, the assessment of the mechanical, thermal properties and tensile tests assisted by digital image correlation (DIC) was performed for curaua fiber MFC-reinforced polylactic acid (PLA) composites as a function of MCF content. First, MFC was incorporated into PLA using a solvent exchange technique and subsequent polymer solubilization to produce master batch composites. Then, more PLA was added to obtain composites with 0.5 and 1.5 wt% MFC by using double screw extrusion and injection molding. As a result, the addition of MFC caused the flexural, tensile, indentation, impact and modulus strengths to increase compared to those of pure PLA. The deformation gradient obtained from DIC verified that the 0.5 wt % MFC/PLA composite presented greater homogeneity in relation to load dispersion, corroborating the higher rigidity, maximum stress, and Poisson's ratio.

1. Introduction

This work aims to contribute to the reduction of the environmental impact of synthetic polymers and the substitution of these materials by biodegradable polymers and their composites [1–3]. For instance, a sustainable alternative is microfibrillated cellulose (MFC)-reinforced polylactic acid (PLA) composites [4].

MFC can be obtained from different sources. The curaua fiber, *Ananas erectifolius*, is a bromeliad plant indigenous of Brazil's Amazon region. The fibers removed from their leaves can reach up to 2 m in length. In Brazil, this plant is used in the production of nets, fishing lines and ropes by the natives [5–10]. Curaua fiber has higher mechanical strength than other natural fibers such as sisal and an alternative fiber which have a modulus and maximum tensile strength of 60 and 90%, respectively [11,12]. Curaua fiber is biodegradable, and its chemical composition is 76.8% cellulose, 15.0% hemicellulose, 6.83% lignin, 0.56% ash and 0.99% other [13]. PLA is obtained from renewable agricultural raw materials that are fermented in lactic acid. It is quite versatile and has high mechanical performance compared to that of polymers such as polyethylene, polypropylene and polystyrene [11, 14–18]), which makes it a promising replacement for nonbiodegradable synthetic polymers.

The MFC in this work was obtained by mechanical defibrillation using a Mazuko mill. This process consists of processing treated fibers in a mill that contains two stones, one static and one rotating. The centripetal forces cause the material to pass through a gap between the stones, which is adjusted so that contact occurs, thus defibrillating the pulp [19,20].

Processing may influence the properties of composites and polymers, changing their mechanical, thermal and dynamic mechanical properties. Drying MFC can be quite problematic due to its tendency to agglomerate and form hydrogen bonds when water sublimation occurs

* Corresponding author. Mechanical Sciences Program, Mechanical Engineering, University of Brasília, Brasília, DF, Brazil.
E-mail addresses: luizquimica@gmail.com (L.C.C. Jesus), monica.janaine@gmail.com (J.M. Oliveira), rosemirandaleao@gmail.com (R.M. Leão), lvrossa@yahoo.com.br (L.R. Beltrami), ademirjzattera@gmail.com (A.J. Zattera), anflor@unb.br (C.T.M. Anflor), doca@unb.br (T.C.R. Doca), sandraluz@unb.br (S.M. Luz).

https://doi.org/10.1016/j.polymertesting.2022.107665
Received 2 June 2022; Accepted 4 June 2022
Available online 8 June 2022

[21,22]. The physical, chemical and mechanical properties of MFC-PLA composites are related to the dispersion of MFC in the PLA polymer matrix: a continuous homogeneous dispersion of MFC within the matrix is of utmost importance [23,24].

Herein, an innovative method called digital image correlation (DIC) will be used to study the influence of MFC on the PLA matrix [25]. This method is an optical technique for measuring material deformation. Despite its recent development, DIC has been successfully used as a tool with high accuracy for measuring surface deformation in the field of experimental solid mechanics by comparing digital surface images of a sample in deformed and undeformed states [26,27]. The technique is widely used for characterizing the mechanical properties (tensile strength, modulus of elasticity and Poisson's ratio) of metallic, polymer and composite materials by coupling with tensile testing [25,28]. Moreover, the compressive strength of a composite can also be severely affected by the concentration of fibers, additives, and reinforcements. This property can be evaluated using standard testing methods (ASTM D695-15) or assessed via indentation tests. In this work, an analysis of the indentation depth produced by a spherical indenter on the different composites is presented.

The determination of the mechanical and thermal properties of composites is relevant to the selection of materials for certain applications. These properties define the behavior of the materials in response to mechanical stresses and temperature since they relate to the ability of a material to resist and transmit these forces without failure or unexpected deformation [19,29]. In this work, flexural, indentation, impact and tensile tests coupled with DIC showed the role of MFC inside PLA. The resulting thermal, morphological and dynamic mechanical properties supported the mechanical property data.

2. Materials and methods

This section describes the procedures for the preparation of the test specimens and the testing methods employed for the characterization of the reference material (pure PLA) and two reinforced configurations.

2.1. Materials

The curaua fibers used in this work were kindly provided by Centro de Apoio a Projetos de Ação Comunitária (CEAPAC), Santarém, PA, Brazil, and had a length of 80 cm. PLA was supplied by GoodFellow, Coraopolis, PA, USA in the form of granules with a diameter of 3 mm, natural color and density of 1.24 g cm^{-3}.

2.2. Preparation of MFC from curaua fibers

The *in natura* fibers were cut into lengths of 25 mm. Then, the samples were immersed in a 2 v/v% NaClO solution for 5 h at a ratio of 15:1 (solution:fiber). After this time, they were washed in distilled water to neutral pH and dried at 25 °C for 48 h and at 60 °C for 12 h in an oven. After drying, the NaClO-treated fibers were immersed in 5 w/v% NaOH solution for 2 h at 50 °C at a ratio of 10:1 (solution:fiber) under manual stirring. After mercerization, the fibers were washed in distilled water to neutral pH and dried at 25 °C for 48 h and at 60 °C for 12 h in an oven [30].

The treated fiber was suspended in water, 3 w/v%, and then MFC was obtained using a Masscolloider Masuko Sangyo mill, model MKCA6-2J. The equipment was coupled to a recirculation pump, and the grinding time was 4 h at a speed of 1500 rpm. The suspension was passed through the mill 200 times (cycles) [19].

2.3. Preparation of the MFC/PLA composites

The solvent exchange process was used to mix MFC with PLA. First, the microfibers prepared as described in section 2.2 were suspended in water, and then chloroform was added to the suspension. Centrifugation was performed to replace the water in the suspension with chloroform. In this way, the MFC was retained by the chloroform. Second, for the solubilization of PLA, 300 mL of chloroform was added to 100 g of powdered PLA. The mixture was incubated for 24 h and then mechanically stirred for 1 h.

The blend with a high concentration of MFC was prepared by a process in which the concentration of the reinforcement material was higher than the final desired value. Then, after mixing, an additional quantity of pure polymer (PLA) was added until the final composite content was reached. To obtain the concentrated mixture, the suspension of MFC and chloroform was first applied to the solubilized polymer in a shaker stirrer for 30 min. The mixture was then subjected to drying at 80 °C for 24 h in an oven from Quimis Scientific Equipments Ltda, B252.

The PLA matrix and the concentrated mixture (PLA + MFC) were ground in a knife mill (Primotecnica, model 1001) and passed through a single-screw extruder (SEIBT, ES 35FR) at temperatures in different heating zones ranging from 120 °C to 185 °C with a thread speed of 150 rpm. The MFC/PLA composites presented fiber contents of 0.5 wt% and 1.5 wt%. Pure polymer (PLA) was processed under the same conditions for subsequent use as reference configuration during the comparative analysis. After that, the materials were ground and subjected to an injection molding process (Himaco, model LHS 150–80) under the same temperature conditions as those used in the extruder to obtain specimens for testing.

2.4. Flexural and impact tests setup

Two-point flexural tests of the polymers and composites were performed in a universal EMIC DL 2000 device following the ASTM D790 standard (ASTM, 2003). The displacement rate used for the test was 1.5 mm/min. The results were collected for five specimens with dimensions of 130 x 15 × 3 mm. Notched specimens with a rectangular cross-section (thickness of 3.2 mm and a width of 10.1 mm) are fixed vertically from the bottom in a CEAST impact machine and subjected to a 2.75 J impact from a pendulum-shaped hammer. Izod impact tests were performed according to ASTM D 256 at 23 °C.

2.5. Tensile tests coupled to DIC setup

Tensile testing was performed on specimens according to the ASTM D638 standard using an Instron 8801 test machine (Instron, Glenview, IL, USA) [±100 kN (22,500 lbf)] with a 2620-601 dynamic gauge extensometer (Instron, Glenview, IL, USA). The Young's modulus, tensile strength, and ultimate tensile strength were determined from the experimental stress-strain curves.

The displacement rate was set to 1 mm/min, and all specimens tested

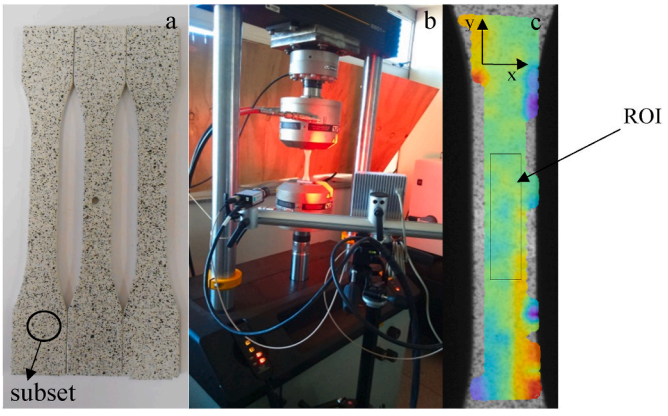

Fig. 1. a) Specimens with a speckle pattern; b) DIC apparatus; and c) Region of interest (ROI) definition for the specimen.

had a speckle pattern generated over the surface with good quality, see Fig. 1a. The accuracy of displacement field assessment by DIC depends on having a good pattern. DIC profiles were taken at 1-s intervals throughout each tensile, as displayed in Fig. 1b. The regions of interest where the strain field was measured during the tensile test are depicted in Fig. 1c.

During tensile testing, a wide range of deformation gradients may occur because MFC is randomly aggregated in the PLA matrix. Accordingly, the Poisson's ratio was determined based on the mean strain inside the rectangular area. The Poisson's ratios for the tested specimens were obtained according to Equation (1) considering the tangential *Lagrangian* mean strain for both the *x* and *y* directions.

$$v = -\frac{\varepsilon_x}{\varepsilon_y} \tag{1}$$

where v is Poisson's ratio and ε_x and ε_y are the strains in the x and y directions (Fig. 1c), respectively.

2.6. Indentation setup

To assess the compression strength of each material configuration, indentation tests have been carried out using a 2.5 mm tungsten carbide spherical indenter mounted in an (ZHU 250) universal indentation system. The indentation marks have been made at the clamping zone of untested tensile specimens, see Fig. 2a.

Before testing, the six specimens (two of each material) have been polished using a metallographic grinding machine (Pantec POLIPAN-U; wet sandpaper discs, four grit stages: 200, 400, 600 and 800, at 300 rpm and 3 min each) and controlled for a 3.60 ± 0.05 mm thickness.

Results for three loads are reported in this study (153.23 N, 306.47 N and 459.69 N), these values were carefully selected after preliminary testing. It's worth mentioning that a load of 61.29 N will lead to indistinguishable results when comparing the indentation marks on the three materials, while a load of 612.92 N will lead to the fracture of 1.5 wt% specimens.

Two indentations (one plus repetition) are made in each one of the specimens to evaluate dispersion. A 3D profile of each indentation mark is obtained using a confocal laser microscope (Olympus LEXT OLS4100; 20x magnification lens with a pitch of 1 μm). Fig. 2b shows a representative profile of an indentation mark. The indentation depth is measured using the microscope's companion software.

2.7. SEM and TEM setup

The specimens were inspected before and after mechanical testing. Before the analyses, the surface of samples was coated with gold using a metallizer for an exposure time of 3 min. SEM analysis was performed on a (SHIMADZU Superscan SS-500) scanning electron microscope with an acceleration voltage of 15 kV. The MFC morphology was analyzed under a transmission electron microscopy technique (JEOL - JEM 2100). Before that, an aqueous suspension with the sample was placed on a carbon grid over a 300-mesh copper sieve. And then, it dried at room temperature, followed by the application of 2% (w/v) of uranyl acetate. Then, the dimensions (length/diameter) of the samples were determined using the ImageJ software in a micrometric precision.

2.8. TGA and DSC setup

Thermogravimetric analysis (TGA) and differential scanning calorimetry (DSC) were performed on a simultaneous TGA-DSC analyzer from TA Instruments, model SDT Q600. The analyses were performed in an alumina crucible with approximately 10–15 mg of sample in a temperature range of 30–500 °C under N_2 atmosphere (flow of 100 mL min^{-1}) with a heating rate of 10 °C.min^{-1}. By using the DSC results, the crystallinity index %Xc was determined using Equation (2).

$$Xc(\%) = \frac{\Delta H_{f\ polymer}}{w.\Delta HF^{\circ}}.100 \tag{2}$$

where $\Delta H_{f\ polymer}$ is the melting enthalpy of the polymer in J.g^{-1}, ΔHF° is the melting enthalpy of the theoretically 100% crystalline polymer, which corresponds to 93.7 J g^{-1} for PLA, and w is the weight percentage of PLA in the composite.

2.9. DMA setup

Tensile specimen samples with rectangular cross section (5 × 4.05 mm) and 25 mm in lenght were used for dynamic mechanical analysis. The equipment used for the test was a PerkinElmer device operating in flexural mode at temperatures from 20 to 150 °C with a heating rate of 3 °C.min^{-1}.

3. Results and discussion

This section presents the findings observed in the experimental data and it is divided in eight subsections covering the different results on mechanical and thermal characterization.

3.1. Flexural and impact testing

Table 1 shows the results of flexural and impact tests for the PLA and composites. The flexural strength results indicated the effective parameters of the bent materials and could thus be used to evaluate the real influence of MFC and therefore the interface between the fibers and the natural matrix based on comparison with PLA. The composites with

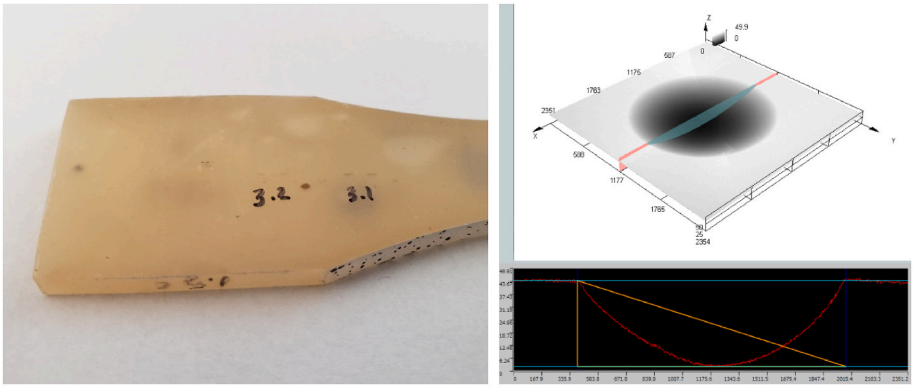

a) b)

Fig. 2. Indentation testing procedure: (a) Placement of the indentation marks, (b) 3D profile of the indentation and depth measurement.

Table 1
Flexural strength limit (FSL), flexural modulus of elasticity (E) and impact strength limit (ISL) of composites and PLA.

Material	FSL (MPa)	E (GPa)	ISL (J.m^{-1})
PLA	42.8 ± 4.74	2.5 ± 0.06	26.0 ± 1.36
0.5 wt% MFC/PLA composite	50.3 ± 2.83	2.8 ± 0.05	26.1 ± 1.52
1.5 wt% MFC/PLA composite	44.0 ± 8.35	2.5 ± 0.18	25.1 ± 1.04

0.5 wt% and 1.5 wt% MFC presented flexural strength results superior to those of the PLA polymer. The composite with 0.5 wt% MFC presented values 17.6% higher than those of PLA. The composite with 1.5 wt% MFC showed no significant improvement. The stiffness of the composites with 0.5 wt% and 1.5 wt% MFC showed an increase of 8.4% and a reduction of 2.6%, respectively, compared to that of PLA.

Regarding the impact test results, there were no significant improvements for the composites compared to PLA. The conservation of these properties by the composites can be attributed to the absorption of impact energy by reinforcement in the polymeric matrix and the consequent reduction in the propagation of microfissures [31].

However, the composites showed an improved flexural modulus of elasticity, but similar improvements were not reflected in the impact results. According to Jonoobi [32], it is expected that polymer composites will present mechanical properties superior to those of the pure PLA, especially in terms of the elastic modulus.

The use of MFC (0.5 wt%) promoted an increase in the modulus of elasticity compared to that of PLA, probably due to the increased stiffness of the samples caused by the addition of MFC. Similar results were also observed in studies by Refs. [14,33,34] that used composites reinforced with MFC. The authors verified that the increase in the modulus of elasticity was justified due to the high degree of crystallinity of the cellulosic material, which made the deformation of the composites difficult. The authors further reported that reinforcement, if evenly dispersed, effectively interacts with the polymer matrix and decreases the space between molecules, decreasing molecular mobility. For Asslan [35], the stiffness of a material is a parameter of great importance for calculating the deformations and vibration modes of a structural component. Therefore, it can be stated that the inclusion of 0.5 wt% MFC in PLA directly influenced the properties of the composite.

3.2. Tensile testing coupled with DIC analysis

The stress-strain curves obtained for PLA, 0.5 wt% MFC/PLA and 1.5 wt% MFC/PLA are presented in Fig. 3. The curve behavior demonstrated that the 0.5 wt% MFC/PLA composite presented a higher tensile strength and deformation than PLA and the 1.5 wt% MFC/PLA composite.

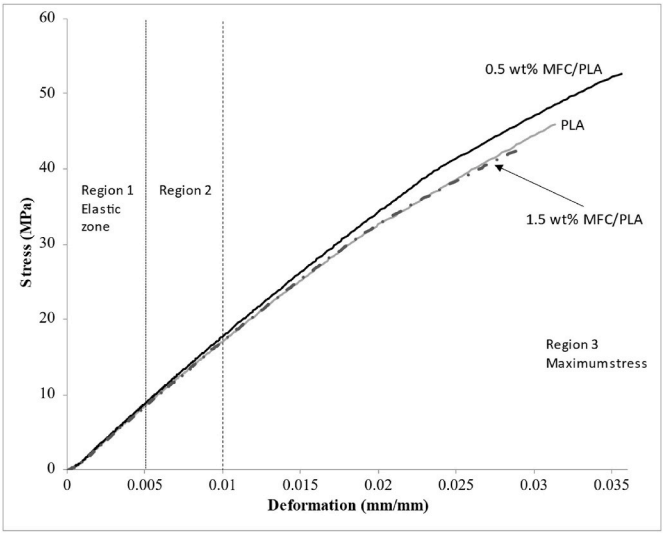

Fig. 3. Tensile strength results of stress-strain curves for the investigated materials.

Table 2 shows the mechanical tensile properties (modulus of elasticity and ultimate tensile stress) obtained from the stress-strain curves (Fig. 3) and from DIC (Poisson's ratio) for PLA and the composites. The mechanical properties were evaluated in three specific regions of the stress-strain curve due to the nonlinear behavior as the load increased, as indicated on Fig. 3 graph. The first region is the elastic zone, the second region is the plastic zone, and the third region is that where the maximum stress is achieved.

According to Table 2, the addition of 0.5 wt% MFC to PLA increased the Poisson's ratio by 10%. An increase, despite being less significant, can also be observed for the 1.5 wt% composite. This increase in lateral contraction resistance suggests that the distribution of MFC improves the composite compared to pure PLA.

The addition of 1.5 wt% MFC resulted in an insignificant improvement in mechanical properties compared with those of PLA. The maximum stress showed an increase of approximately 1% for region #1, 30% for region #2 and 18% for region #3. The maximum stress presented an approximately 1% increase for regions #1 and #2, while no influence on the mechanical properties is observed for region #3.

According to Farah et al. [36], the Poisson's ratios for PLA and its derivatives are equal to 0.3, and their rigidity is related to their semi-crystalline structure, similar to the results of this paper. It is worth noting that the present result for the Poisson's ratio of PLA (0.39 ± 11) is in good agreement. In addition, Farah et al. [36] corroborated that the Poisson's ratio for most fragile polymers is approximately 0.36.

Fig. 4 illustrates the evolution of the tensile tests using the images provided by the DIC system. Fig. 4 (a) presents the gradients of the displacements before rupture stress, while Fig. 4 (b) presents the fractured specimens. Each specimen mapping was performed over the ROI shown in Fig. 4 with a color scale representing the values of the displacements and deformations along the axis of stress. From the displacement field and following the expected behavior of the tensile test, one can observe that in the upper part remained restrained, while the lower part undergoes a maximum displacement of approximately 2 mm in the moment of rupture. On the other hand, in the deformation field, the specimen does not present appreciable lateral restriction at the instant of rupture.

From the deformation gradient, it was noted that the material with 0.5 wt% MFC presented the greatest homogeneity in relation to the load

Table 2
Mechanical properties for PLA and 0.5 wt% and 1.5 wt% MFC/PLA composites for the three ROIs according to tensile testing coupled with DIC.

Property	Material/ Region	PLA	0.5 wt% MFC/PLA	1.5 wt% MFC/PLA
Poisson's ratio	Region #1	0.39 ± 0.11	0.52 ± 0.07	0.42 ± 0.07
	Region #2	0.47 ± 0.15	0.52 ± 0.14	0.47 ± 0.13
	Region #3	0.36 ± 0.23	0.42 ± 0.17	0.35 ± 0.09
Maximum strength (MPa)	Region #1	8.77 ± 0.17	8.89 ± 0.12	8.74 ± 0.23
	Region #2	13.56 ± 0.31	17.76 ± 0.08	17.62 ± 0.33
	Region #3	44.34 ± 0.41	52.71 ± 0.11	44.22 ± 1.41
Modulus of elasticity (GPa)	Region #1	2.72 ± 61.98	2.77 ± 25.04	2.74 ± 50.31
	Region #2	2.72 ± 66.66	2.76 ± 8.99	2.75 ± 37.14
	Region #3	2.51 ± 13.59	2.53 ± 44.32	2.51 ± 73.91

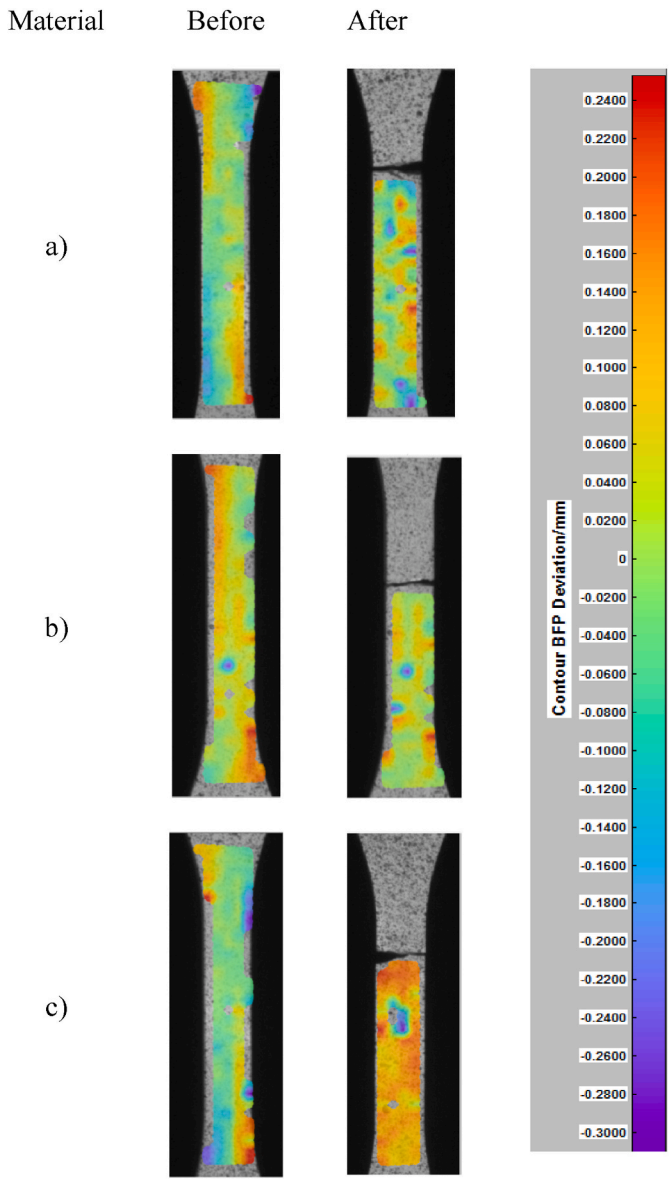

Fig. 4. DIC results for (a) PLA, (b) 0.5 wt% MFC/PLA and (c) 1.5 wt% MFC/PLA composites immediately before and after fracture.

dispersion. This fact is confirmed by the thermal, mechanical, dynamic-mechanical and morphological properties, which strongly influence the mechanical properties, corroborating the higher stiffness, maximum tension and Poisson's ratio of the composite in comparison to those of PLA and supporting the results presented in Table 2.

The deformation gradient is presented with a color scale and represents the specimen behavior while undergoing deformation. Analysis of the DIC results verified the field of displacement that occurred on the surface of the materials. Producing a random pattern on the surface of a material is essential for the collection of satisfactory data by this procedure. To create this pattern on our samples, spray paint has been used.

When MFC is randomly aggregated into a PLA matrix, the fibers absorb fracture energy due to different crack angles. According to Zhang et al. [37], DIC provides surface images of a material and can display the microcharacteristics of composites for qualitative analysis. However, it is difficult to observe profiles of damaged materials. In the current application, the main benefit is that the technique not only provides material deformation contours (obtained directly from deformed images) but also provides a quantitative description of the stress distribution of the materials. The authors state that fractures generated from mechanical stress in composite materials can generate aggregate detachment by dissipating heat via the interface. According to He et al. [38], the DIC technique completely measures the deformation field and is comparable to other computational or even experimental techniques, being even more accurate than these other techniques.

3.3. Indentation results

The 36 individual measurements of indentation depth are listed in Table 3 and depicted in Fig. 5. Results show a linear trend (98% agreement) and a low dispersion at all tested conditions.

The 0.5 wt% MFC/PLA configuration displays the lowest values of indentation depth: when compared to the pure PLA (reference condition), its results are −8%, −14% and −13% at the respective loads of 153.23 N, 306.47 N and 459.69 N. This infers that the addition of 0.5 wt % MFC to the PLA matrix leads to a higher compressive strength at these tested conditions.

However, an increase of MFC to 1.5 wt% leads to deeper (+3%, +2% and +8%) indentation marks. This behavior can represent a loss in stiffness due to what it seems to be an excessive amount of MFC in the PLA matrix. Therefore, the indentation tests results have corroborated the observations made in the previous analyses.

3.4. TEM of MFC and SEM of composites and PLA

The fractured surfaces of PLA and the composites were investigated by SEM to evaluate the influence of the addition of MFC on the PLA microstructure. A transmission electron microscopy (TEM) of MFC before being incorporated into the natural matrix and an image of PLA are presented in Fig. 6 (a) and (b), respectively, for comparison with the composites.

Fig. 6 (b) shows the morphology of the PLA matrix and the presence of cracks, probably due to stresses resulting from the injection process and the mechanical stress applied to the material in the mechanical tensile test. Fig. 6 (c) and (d) indicate a good reinforcement distribution in the natural matrix. There was a reasonable interaction between the fibers and the matrix, as well as removal of the fibers from the matrix. Also, it is observed from Fig. 6 that the dispersed fiber in the PLA matrix has a diameter of approximately 276 nm, demonstrating that it remained in the microstate and thus increased the contact surface between the fiber and the matrix.

The difference between MFC before and after the PLA matrix was added indicates that during the master batch production process, no MFC agglomeration occurred, demonstrating that the process was effective to produce the composite material. The composites were also found to be materials with reasonable homogeneity, as evidenced by the improvements in mechanical properties.

Lopera-Valle et al. [39] and Vestena et al. [40], obtained a film sample from a PLA nanocomposite reinforced with cellulose nanocrystals and found that more homogeneous materials have more effective plastic deformation, a fact also indicated in the DIC analysis of region 2 (plastic zone), as indicated at Fig. 3.

The composites presented a low micropore content, as shown in Fig. 6 (c) and (d). It is noteworthy that usually, the smaller the number of micropores is, the better the mechanical properties of the composite. The presence of micropores in the polymeric matrix at an amount above 20% by volume is probably responsible for decreasing the mechanical resistance. Micropores often act as defects, reducing the load carrying capacity and energy absorption capacity of the composite [31,41].

Fig. 6 (b) and (d) show that MFC-reinforced composites have reasonable adhesion between the microfibers and the matrix, as the reinforcement is not "loose", suggesting that they ruptured during the tensile test. The occurrence of fracture propagation around the fibers is also noted. Cellulosic fibers have cellular arrangements that can modify the path of cracks. Therefore, in the fiber composites, the cracks do not have a straight trajectory because they travel around the fiber cells and

Table 3
Indentation test results, depth [μm] versus normal force [N].

Force	PLA				0.5 wt% MFC/PLA				1.5 wt% MFC/PLA			
	Specimen 1		Specimen 2		Specimen 1		Specimen 2		Specimen 1		Specimen 2	
	Depth 1	Depth 2	Depth 1	Depth 2	Depth 1	Depth 2	Depth 1	Depth 2	Depth 1	Depth 2	Depth 1	Depth 2
153.23	11.960	12.152	12.080	12.005	11.120	11.185	11.096	11.065	12.552	11.679	12.785	12.578
306.47	27.322	25.306	26.563	25.942	22.790	22.652	22.116	22.430	26.419	26.548	26.939	26.907
459.69	47.946	47.941	49.076	48.216	44.109	40.928	40.620	42.033	47.401	53.811	53.004	54.966

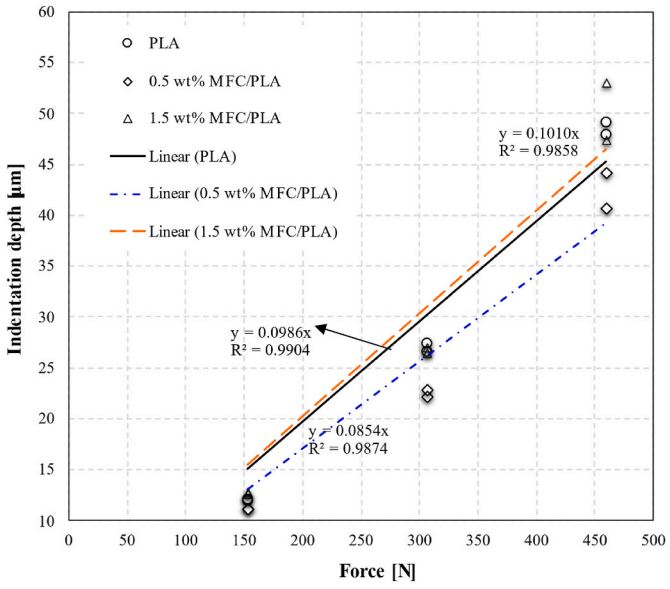

Fig. 5. Indentation depth results, trendlines and coefficients of determination for the three material configurations.

finally cease [42].

3.5. Characterization of PLA and composites by TG

Thermal degradation and stability were determined by thermogravimetry (TG)/derivative thermogravimetry (DTG) curves. This technique can be used to evaluate the temperature limit at which a material can be processed and the influence of the MFC content in the PLA polymer matrix. The thermal behaviors of PLA and the composites were also studied. This analytical approach is generally used to assess the level of thermal stability of samples. Fig. 7 shows the TG/DTG curves of MFC, PLA and the composites.

From the TG curves, it was found that for the PLA composites with MFC and the PLA polymer, the maximum temperature of thermal stability was 270 °C, an intermediate temperature between the maximum values for MFC and the PLA matrix. Differences in thermal behavior between the composite materials, MFC, and polymer can be easily visualized from the DTG curve.

Borsoi et al. [43] observed the behavior of cellulosic materials at temperatures below and above 300 °C. They stated the temperature conditions in which cellulose is exposed to thermal degradation. Below 300 °C, degradation reactions are mainly attributed to water dehydration and peroxide formation, which can catalyze cellulose degradation. Degradation reactions below 300 °C are slow, and complete degradation of cellulose under these conditions may involve a slow reaction. Above 300 °C, the degradation mechanism differs mainly over time and is considered a rapid degradation reaction. At this temperature, hydrogen bonds break, forming free radicals and carbonyl and carboxyl groups, which accelerate the primary degradation of cellulose. Between 310 and 390 °C, three hydrolysis products are formed: tar (or a fraction of heavy oil that vaporizes at higher temperatures), ash and condensable and noncondensable gases. These products are the result of a series of transglycosidations and dehydration reactions.

According to Fig. 7, PLA shows a weight loss T_{onset} of 265 °C, the 1.5 wt% MFC/PLA composite has a T_{onset} of 256.4 °C, and 0.5 wt% MFC/PLA shows a T_{onset} of 273 °C. The maximum degradation peaks were 354 °C for PLA, 353 °C for the composite with 0.5 wt% MFC and 356 °C for the material with 1.5 wt% MFC. The material loss was 99.23% for PLA, 98.64% for the 0.5% MFC-reinforced material and 98.0% for the 1.5 wt% MFC-reinforced material. Similar results were also evidenced in a study by Rizal et al. [44]: in the TG curves of carbon nanoparticle-reinforced PLA, the presence of three weight loss events was observed, suggesting that the material had more than one component with different degradation temperatures.

From the TG and DTG curves, the composites degraded at temperatures similar to that of PLA. According to Rizal et al. [44], although the thermal degradation of MFC components occurs at temperatures below that of PLA, the load quantity did not reduce the thermal stability of the materials. The percentages of weight loss at temperatures from 100 to 400 °C for the composites, polymer and MFC. In the composites, the weight loss was practically the same as that of the material without the addition of MFC. Thus, by comparing the polymer and composites, it can be stated that the addition of MFC assisted in preserving the thermal stability of the composites compared to that of PLA.

3.6. DSC of MFC, PLA and composites

The results of DSC thermal analyses of PLA, the composites and MFC are shown in Fig. 8 and Table 4. The DSC curves for PLA and the composites yielded three characteristic events. The typical event at approximately 65 °C corresponds to the glass transition temperature (T_g) of the materials. The event at approximately 170 °C is related to the melt temperature (T_m) of the PLA matrix. Finally, the peak at 365 °C corresponds to the thermal degradation of the materials. Similarly, Murariu and Dubois [45] developed PLA and natural fiber-based polymer composites and found PLA T_g values ranging from 50 °C to 80 °C and T_m values ranging from 130 °C to 180 °C.

According to Fig. 8 and Table 4, in MFC, two thermal events are observed, the first (before 100 °C) attributed to the water vaporization heat and the second to cellulose degradation (before 400 °C). As the cellulose fiber underwent pretreatment and milling processes, the second thermal event is unlikely to correspond to the fusion of lignin or cellulose oligomers. This peak may correspond to the rupture of inter- and intramolecular hydrogen bonds, probably involving the cellulosic structure, or possibly resulting from accommodation involving the crystalline regions of cellulose causing changes in the type of crystal lattice [46,47].

Regarding the crystallinity index (Xc), as we can see in Table 4, there was an increase in Xc for all composites compared to that of PLA. It is worth mentioning the increase in crystallinity of the material reinforced with 0.5 wt% MFC (Xc = 34.24%) compared to that of pure PLA was probably associated with greater restriction of the movement of polymer chains promoted by MFC. Sena Neto et al. [48], obtained and characterized curaua fiber-reinforced composites and found an increase in the crystallinity of the composites compared to that of PLA. According to

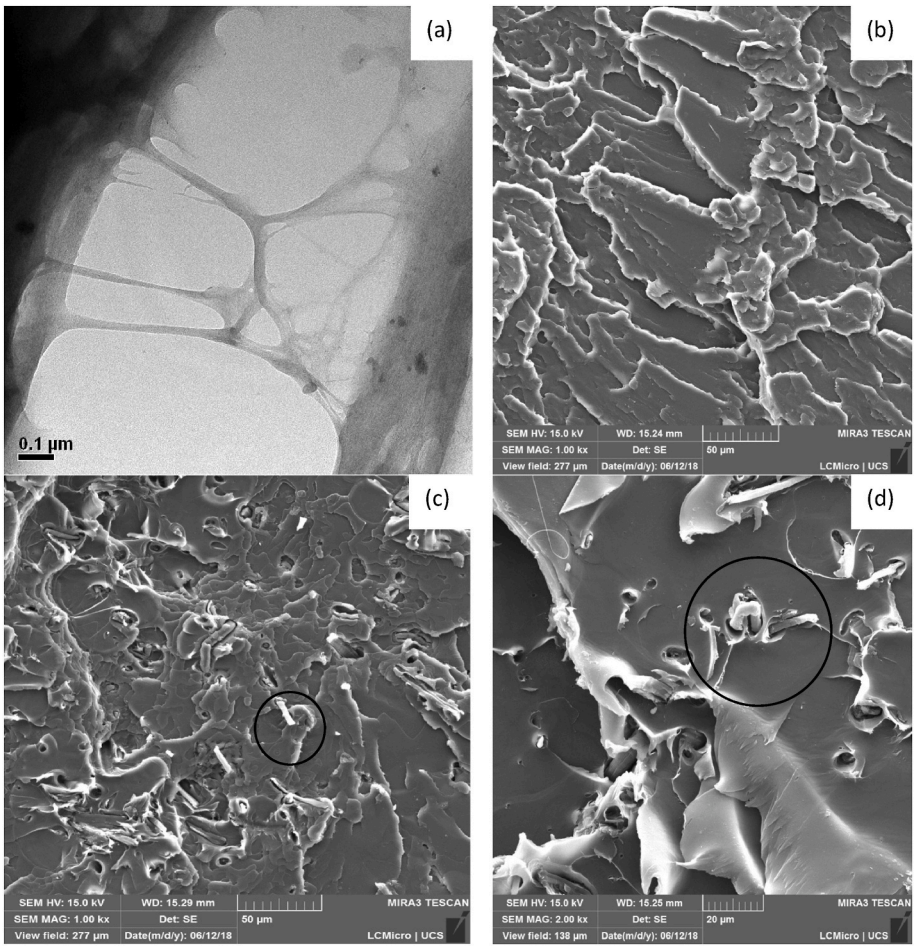

Fig. 6. Transmission electron microscopy (TEM) of MFC before being incorporated into the natural matrix (a); SEM images for PLA matrix (b) and PLA composite with 1000 x magnification (c) and 2000 x magnification (d).

Murariu and Dubois [45], fibers can act as nucleating agents restricting the movement of carbon chains, increasing the crystallinity of composites.

3.7. DMA results

DMA tests were performed for PLA and the composites to verify the viscoelastic behavior, storage modulus, loss modulus and tan δ as a function of temperature, frequency or time. The mechanical dynamic behavior of heterogeneous systems such as composites depends on factors such as composition, phase morphology, phase adhesion and individual component properties [49].

The behavior of the storage modulus for the polymer and composites is presented in Fig. 9. There was an increase in storage modulus (E′) with the addition of MFC. This behavior is associated with the increased molecular restriction imposed by the addition of MFC to the biodegradable matrix. The MFC composites showed a higher E′ than did PLA. The composite with 0.5 wt% MFC showed an increase in E' due to the reasonable adhesion between MFC and the polymeric matrix and the presence of micropores in the polymeric matrix. Such adhesion was proven by SEM analyses by Spinella et al. [50], who found similar behavior in a cellulose nanocrystal-reinforced PLA nanocomposite film, with the load ranging from 0 to 20% by weight. They found that the material with a 5 wt% nanocrystal loading had a 450% increase in storage modulus over that of pure PLA.

The variation in tan δ as a function of temperature for PLA and the composites is shown in Fig. 9b. With the addition of MFC, there was a small reduction in the height of the tan δ peak. According to Lorandi et al. [51], the energetic evaluations of composites are related to the height of the tan δ peak. The more intense the fiber/polymer matrix interaction is, the lower the energy dissipation and the lower the tan δ peak height since energy release in the composites occurs via the interface [50]. In the analyzed composites, there was a reduction in the degree of damping in relation to that of PLA. With the addition of MFC, the amount of polymer matrix decreased, and the degree of damping increased. The value of tan δ indicates polymer chain movement and quantifies the interaction between the microfiber and matrix. Tan δ indicates the relaxation capacity of a material, i.e., the mechanical strength. This restriction of the movement of polymer matrix chain segments resulted in a slight increase in the storage modulus for the 0.5 wt% MFC composite over that of PLA.

T_g is related to tan δ and is the temperature where the value of tan δ is maximum, but it can also be defined as the temperature where the value of E″ is maximum or the temperature where the highest change in E′ occurs. The intersection point of the E′ and E″ curves can also be used to estimate the T_g of these types of materials. Rezaei et al. [52], realized this relationship in their study on the dynamic mechanical properties of carbon fiber-reinforced polypropylene composites.

Polymer composites have physical, chemical and mechanical properties that are highly influenced by temperature. For semicrystalline polymer matrix composites, as in the case of PLA, T_g is of paramount importance since below T_g, the movement of the polymer matrix chains is restricted, while above T_g, the composites acquire satisfactory mobility so that many chains act jointly, and changes in carbon conformation occur [53]. The presence of a stiffer phase, such as cellulose microfibers, can facilitate the displacement of T_g from the plastic

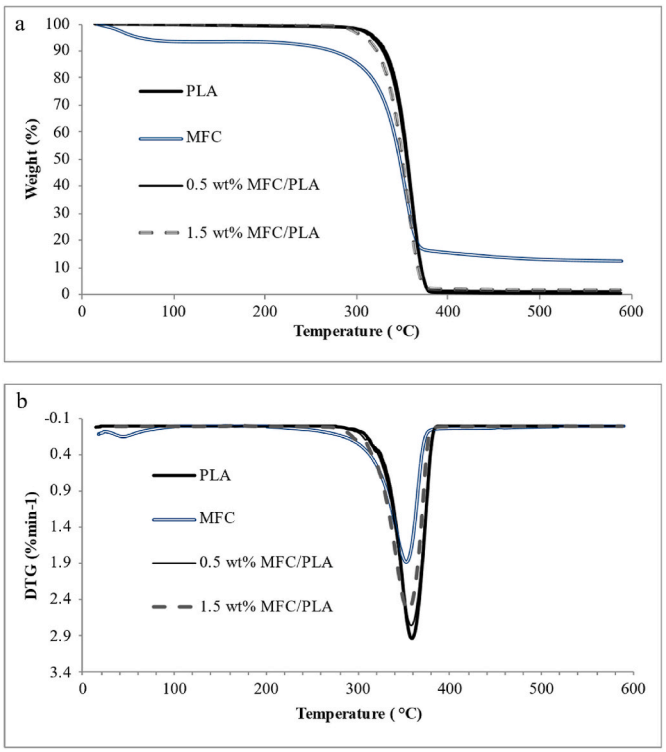

Fig. 7. a) TG and b) DTG curves of PLA, MFC and composites.

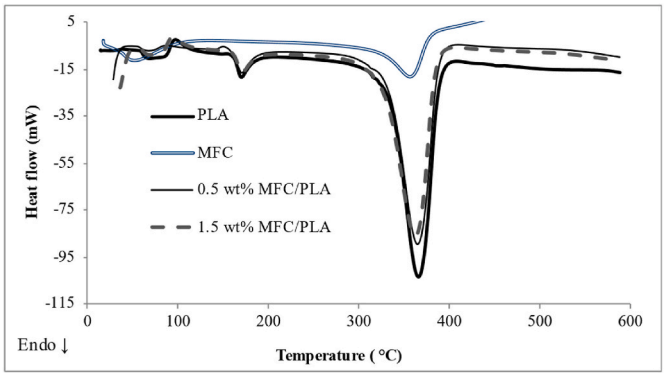

Fig. 8. DSC curves for PLA and MFC/PLA composites.

region to higher values. Increased stiffness is caused due to percolation between the cellulose microfiber and the PLA polymer matrix.

When a good microfiber/matrix interaction occurs, there are restrictions on the movement of carbon chains at the fiber interface, causing a reduction in T_g and a decrease in the degree of damping, as can be observed in the T_g values obtained at the temperature associated with the peak of tan δ, which are given by Table 5. The literature Borsoi et al. [53], states that T_g for PLA is 60.8 °C, showing that the obtained values are within the expected range. The presence of MFC tends to anchor the polymeric chain, necessitating a higher energy expenditure for the chain to become mobile and increasing the T_g of composites proportionally to their volume [21].

Table 5 shows a comparison of the dynamic modulus and tan δ between PLA and the composites. The E′, E″ and tan δ modulus indicate changes in conformation in the carbon chains of the polymeric materials. However, these parameters are directly related to structure, molecular mass and atom types. The MFC composites showed a higher modulus of elasticity due to the addition of MFC to the PLA matrix. The storage modulus of the composites with 0.5 wt% MFC was increased by 16% compared to that of PLA. The addition of MFC to the natural PLA matrix caused the composites to become more rigid due to distribution between the MFC and the matrix, a fact proven in the mechanical test.

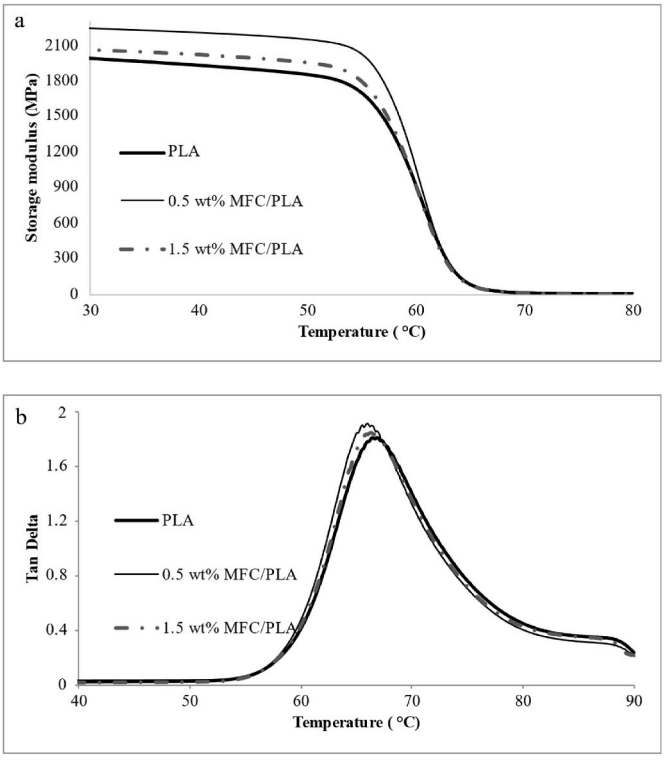

Fig. 9. a) Storage modulus (E′) and b) tan δ for PLA and composites.

Table 5
Dynamic mechanical properties of composites and polymer.

Materials	E′ at 50 °C (MPa)	E'' at 60 °C (MPa)	Tan δ at 65 °C	T_g at tan δ peak (°C)
PLA	1844.6	376.0	1.8	60.2
0.5 wt% MFC/PLA	2139.9	485.3	1.9	61.0
1.5 wt% MFC/PLA	1954.5	414.5	1.8	59.1

Table 4
Crystallinity index and enthalpy events from the DSC curves for PLA and the composites.

Sample	Crystallinity index (%)	Thermal events Temperature (°C)/Enthalpy ΔH (J/g)					
		First		Second		Third	
PLA	28.91	57.2	17.2	170.0	29.2	365.8	1070.0
MFC	–	64.0	327.5	349.1	575.6	–	–
0.5 wt% MFC/PLA	34.24	58.3	19.1	170.3	52.0	364.7	923.6
1.5 wt% MFC/PLA	31.9	53.6	15.1	170.9	39.2	362.4	834.9

4. Conclusions

PLA composites with 0.5 wt% MFC showed better mechanical, indentation, flexural and dynamic mechanical properties than pure PLA. In the impact test, the properties remained comparable to those of PLA. These results indicate better matrix transfer to the microfibers due to the improved interface. From the DIC results, according to the deformation gradient, the material with 0.5 wt% MFC presented greater homogeneity in relation to the load dispersion. The indentation tests revealed that an addition of 1.5 wt% of MFC lead to the deeper marks. The thermal, mechanical, dynamic-mechanical and morphological properties strongly influenced the mechanical properties, corroborating the higher rigidity, maximum stress and Poisson's ratio in relation to those of PLA.

In the 1.5 wt% MFC-reinforced material, there was no improvement in dynamic mechanical properties, probably due to the agglomeration of fibers, causing them to act as stress concentrators. The composites showed a small reduction in tan δ peak height according to the MFC content. The hydrophilic groups present in the MFC and the PLA matrix promoted the reduction in the tan δ peak due to the reduction in friction between MFC and the matrix in the interface region. The composites reinforced with cellulosic fibers showed low thermal stability.

Declaration of competing interest

The authors declare that they have no known competing financial interests or personal relationships that could have appeared to influence the work reported in this paper.

Acknowledgements

The authors would like to thank Coordenação de Aperfeiçoamento de Pessoal de Nível Superior (CAPES), Decanato de Pós Graduação/University of Brasília (DPG/UnB), and Fundação de Apoio à Pesquisa do Distrito Federal (FAPDF) under the projects N° 0193.001.554/2017 and 0193.001794/2017, as well as Conselho Nacional de Desenvolvimento Científico (CNPq).

References

[1] V.C. Brambilla, L.V.R. Beltrami, K. Pelegrini, M.V.G. Zimmermann, R. N. Brandalise, A.J. Zattera, Development and characterization of PLA/buriti fibre composites - influence of fibre and coupling agent contents, Polym. Polym. Compos. 25 (2017) 143–152, https://doi.org/10.1177/096739111702500204.

[2] R.M. Leão, P.C. Miléo, J.M.L.L. Maia, S.M. Luz, Environmental and technical feasibility of cellulose nanocrystal manufacturing from sugarcane bagasse, Carbohydr. Polym. 175 (2017) 518–529, https://doi.org/10.1016/j.carbpol.2017.07.087.

[3] R. Zhang, H. Hu, Y. Liu, J. Tan, W. Chen, C. Ying, Q. Liu, X. Fu, S. Hu, C.P. Wong, Homogeneously dispersed composites of hydroxyapatite nanorods and poly(lactic acid) and their mechanical properties and crystallization behavior, Composer Part A Appl. Sci. Manuf. 132 (2020), https://doi.org/10.1016/j.compositesa.2020.105841.

[4] J.H. Jang, S.H. Lee, T. Endo, N.H. Kim, Dimension change in microfibrillated cellulose from different cellulose sources by wet disk milling and its effect on the properties of PVA nanocomposite, Wood Sci. Technol. 49 (2015) 495–506, https://doi.org/10.1007/s00226-015-0703-2.

[5] C.P.F. Souza, E.H. de Souza, C.A. da S. Ledo, F.V.D. Souza, Evaluation of the micropropagation potential of Curauá pineapple hybrids for fiber production, Acta Amazonica 48 (2018) 290–297, https://doi.org/10.1590/1809-4392201800382.

[6] R. Motta Neves, K. Silveira Lopes, M.G.V. Zimmermann, M. Poletto, A.J. Zattera, Cellulose nanowhiskers extracted from tempo-oxidized curaua fibers, J. Nat. Fibers 17 (2020) 1355–1365, https://doi.org/10.1080/15440478.2019.1568346.

[7] J.P. De Mesquita, C.L. Donnici, F.V. Pereira, Biobased nanocomposites from layer-by-layer assembly of cellulose nanowhiskers with chitosan, Biomacromolecules 11 (2010) 473–480, https://doi.org/10.1021/bm9011985.

[8] A.L. Pereira, M.D. Banea, J.S.S. Neto, D.K.K. Cavalcanti, Mechanical and thermal characterization of natural intralaminar hybrid composites based on sisal, Polymers 12 (2020), https://doi.org/10.3390/POLYM12040866.

[9] A. Sivoney, F. Souza, M. Mariano, M. Sain, Cell interactions and cytotoxic studies of cellulose nanofibers from curauá natural fibers, Carbohydr. Polym. 201 (2018) 87–95.

[10] F. Tomczak, K.G. Satyanarayana, T.H.D. Sydenstricker, Studies on lignocellulosic fibers of Brazil: Part III - morphology and properties of Brazilian curauá fibers, Composer Part A Appl. Sci. Manuf. 38 (2007) 2227–2236, https://doi.org/10.1016/j.compositesa.2007.06.005.

[11] V.H. Orozco, W. Brostow, W. Chonkaew, B.L. López, Preparation and characterization of poly(Lactic Acid)- G-maleic anhydride + starch blends, Macromol. Symp. 277 (2009) 69–80, https://doi.org/10.1002/masy.200950309.

[12] T.y.Y.G. Girijappa, S. Mavinkere Rangappa, J. Parameswaranpillai, S. Siengchin, Natural fibers as sustainable and renewable resource for development of eco-friendly composites: a comprehensive review, Front. Mater. 6 (2019) 1–14, https://doi.org/10.3389/fmats.2019.00226.

[13] O. Faruk, A.K. Bledzki, H. Fink, M. Sain, Progress in polymer science biocomposites reinforced with natural fibers : 2000 – 2010, Prog. Polym. Sci. 37 (2012) 1552–1596, https://doi.org/10.1016/j.progpolymsci.2012.04.003.

[14] J. Yang, Y.C. Ching, C.H. Chuah, Applications of lignocellulosic fibers and lignin in bioplastics: a review, Polymers 11 (2019) 1–26, https://doi.org/10.3390/polym11050751.

[15] J.M.F. Silva, B.G. Soares, Epoxidized cardanol-based prepolymer as promising biobased compatibilizing agent for PLA/PBAT blends, Polym. Test. 93 (2021) 4–10, https://doi.org/10.1016/j.polymertesting.2020.106889.

[16] C.M. Chan, L.J. Vandi, S. Pratt, P. Halley, D. Richardson, A. Werker, B. Laycock, Composites of wood and biodegradable thermoplastics: a review, Polym. Rev. 58 (2018) 444–494, https://doi.org/10.1080/15583724.2017.1380039.

[17] D. Puspita, L. Musyarofah, E. Hidayah, Sujito, Fabrication and tensile properties of bamboo micro-fibrils (BMF)/poly-lactic acid (PLA) green composite, J. Phys. Conf. Ser. 1217 (2019), https://doi.org/10.1088/1742-6596/1217/1/012005, 0–9.

[18] N. Graupner, A.S. Herrmann, J. Müssig, Natural and man-made cellulose fibre-reinforced poly(lactic acid) (PLA) composites: an overview about mechanical characteristics and application areas, Composer Part A Appl. Sci. Manuf. 40 (2009) 810–821, https://doi.org/10.1016/j.compositesa.2009.04.003.

[19] M.V.G. Zimmermann, C. Borsoi, A. Lavoratti, M. Zanini, A.J. Zattera, R.M. C. Santana, Drying techniques applied to cellulose nanofibers, J. Reinforc. Plast. Compos. 35 (2016) 682–697, https://doi.org/10.1177/0731684415626286.

[20] C. Adu, L. Berglund, K. Oksman, S.J. Eichhorn, M. Jolly, C. Zhu, Properties of cellulose nanofibre networks prepared from never-dried and dried paper mill sludge, J. Clean. Prod. 197 (2018) 765–771, https://doi.org/10.1016/j.jclepro.2018.06.263.

[21] R.M. Leão, L.C.C. Jesus, P.T. Bertuoli, M.L.L. Maia, C. Henrique, S. Menezzi, S. C. Amico, S.M. Luz, Production and characterization of cellulose nanocrystals/acrylonitrile butadiene styrene nanocomposites, J. Compos. Mater. (2020) 8, https://doi.org/10.1177/0021998320927773, 0(0).

[22] V. Khoshkava, M.R. Kamal, Effect of drying conditions on cellulose nanocrystal (CNC) agglomerate porosity and dispersibility in polymer nanocomposites, Powder Technol. 261 (2014) 288–298, https://doi.org/10.1016/j.powtec.2014.04.016.

[23] S. Sousa, A. Costa, A. Silva, R. Simões, Poly(lactic acid)/Cellulose films produced from composite spheres prepared by emulsion-solvent evaporation method, Polymers 11 (2019) 1–19, https://doi.org/10.3390/polym11010066.

[24] K. Okubo, T. Fujii, E.T. Thostenson, Multi-scale hybrid biocomposite: processing and mechanical characterization of bamboo fiber reinforced PLA with microfibrillated cellulose, Composer Part A Appl. Sci. Manuf. 40 (2009) 469–475, https://doi.org/10.1016/j.compositesa.2009.01.012.

[25] E. Romeo, Two-dimensional digital image correlation for asphalt mixture characterisation: interest and limitations, Road Mater. Pavement Des. 14 (2013) 747–763, https://doi.org/10.1080/14680629.2013.815128.

[26] M.B.A.M. Oberg, D.F. de Oliveira, J.N.V. Goulart, C.T.M. Anflor, A novel to perform a thermoelastic analysis using digital image correlation and the boundary element method, Int. J. Mech. Mater. Eng. 15 (2020) 1–13, https://doi.org/10.1186/s40712-019-0115-4.

[27] A. Villarino, J. López-Rebollo, N. Antón, Analysis of mechanical behavior through digital image correlation and reliability of pinus halepensis mill, Forests 11 (2020) 1–23, https://doi.org/10.3390/f11111232.

[28] A.H.A. Santos, R.L.S. Pitangueira, G.O. Ribeiro, R.B. Caldas, Study of size effect using digital image correlation, RIEM - IBRACON Struct. Mater. J. 8 (2015) 323–331.

[29] A.G. Adeniyi, D.V. Onifade, J.O. Ighalo, A.S. Adeoye, A review of coir fiber reinforced polymer composites, Compos. B Eng. 176 (2019), https://doi.org/10.1016/j.compositesb.2019.107305.

[30] J.M. de Oliveira, Obtaining and Characterizing Biodegradable Lactic Polyacid (PLA) Composites Reinforced with Curauá Fibers, University de Brásília, 2016.

[31] R.M. Di Benedetto, E.C. Botelho, G.F. Gomes, D.M. Junqueira, A.C. Ancelotti Junior, Impact energy absorption capability of thermoplastic commingled composites, Compos. B Eng. 176 (2019), https://doi.org/10.1016/j.compositesb.2019.107307.

[32] M. Jonoobi, A.P. Mathew, K. Oksman, Producing low-cost cellulose nanofiber from sludge as new source of raw materials, Ind. Crop. Prod. 40 (2012) 232–238, https://doi.org/10.1016/j.indcrop.2012.03.018.

[33] J.M. Lagarón, A. López-Rubio, M. José Fabra, Bio-based packaging, J. Appl. Polym. Sci. 133 (2016), https://doi.org/10.1002/app.42971.

[34] B.E.B. Uribe, A.J.F. Carvalho, J.R. Tarpani, Low-cost, environmentally friendly route to produce glass fiber-reinforced polymer composites with microfibrillated cellulose interphase, J. Appl. Polym. Sci. 133 (2016) 1–9, https://doi.org/10.1002/app.44183.

[35] M. Asslan, Factors influencing small-strain stiffness of soils and its determination, term pap, Bauhaus 1 (2008) 70.

[36] S. Farah, D.G. Anderson, R. Langer, Physical and mechanical properties of PLA, and their functions in widespread applications — a comprehensive review, Adv. Drug Deliv. Rev. 107 (2016) 367–392, https://doi.org/10.1016/j.addr.2016.06.012.

[37] J. Zhang, C. Xiong, H. Li, M. Li, J. Wang, J. Fang, Damage and fracture evaluation of granular composite materials by digital image correlation method, Acta Mech. Sin. Xuebao. 20 (2004) 408–417, https://doi.org/10.1007/bf02489379.
[38] Y. He, A. Makeev, B. Shonkwiler, Characterization of nonlinear shear properties for composite materials using digital image correlation and finite element analysis, Compos. Sci. Technol. 73 (2012) 64–71, https://doi.org/10.1016/j.compscitech.2012.09.010.
[39] A. Lopera-Valle, J.V. Caputo, R. Leão, D. Sauvageau, S.M. Luz, A. Elias, Influence of epoxidized Canola Oil (eCO) and Cellulose Nanocrystals (CNCs) on the mechanical and thermal properties of polyhydroxybutyrate (PHB)-Poly(lactic acid) (PLA) blends, Polymers 11 (2019), https://doi.org/10.3390/polym11060933.
[40] M. Vestena, I.P. Gross, C.M.O. Müller, A.T.N. Pires, Nanocomposite of poly(lactic acid)/cellulose nanocrystals: effect of CNC content on the polymer crystallization kinetics, J. Braz. Chem. Soc. 27 (2016) 905–911, https://doi.org/10.5935/0103-5053.20150343.
[41] L.Y. Molefe, N.M. Musyoka, J. Ren, H.W. Langmi, P.G. Ndungu, R. Dawson, M. Mathe, Synthesis of porous polymer-based metal–organic frameworks monolithic hybrid composite for hydrogen storage application, J. Mater. Sci. 54 (2019) 7078–7086, https://doi.org/10.1007/s10853-019-03367-1.
[42] Z. Zhu, M. Hao, N. Zhang, Influence of contents of chemical compositions on the mechanical property of sisal fibers and sisal fibers reinforced PLA composites, J. Nat. Fibers 17 (2020) 101–112, https://doi.org/10.1080/15440478.2018.1469452.
[43] C. Borsoi, H.L. Ornaghi, L.C. Scienza, A.J. Zattera, C.A. Ferreira, Isolation and characterisation of cellulose nanowhiskers from microcrystalline cellulose using mechanical processing, Polym. Polym. Compos. 25 (2017) 563–570, https://doi.org/10.1177/096739111702500801.
[44] S. Rizal, F.G. Olaiya, N.I. Saharudin, C.K. Abdullah, N.G. Olaiya, M.K. Mohamad Haafiz, E.B. Yahya, F.A. Sabaruddin, Ikramullah, H.P.S. Abdul Khalil, Isolation of textile waste cellulose nanofibrillated fibre reinforced in polylactic acid-chitin biodegradable composite for green packaging application, Polymers 13 (2021) 1–15, https://doi.org/10.3390/polym13030325.
[45] M. Murariu, P. Dubois, PLA composites: from production to properties, Adv. Drug Deliv. Rev. 107 (2016) 17–46, https://doi.org/10.1016/j.addr.2016.04.003.
[46] A.L. de Lemos, P.G.P. Pires, M.L. de Albuquerque, V.R. Botaro, J.M.F. de Paiva, N. S. Domingues Junior, Biocomposites reinforced with natural fibers: thermal, morphological and mechanical characterization, Rev. Mater. 22 (2017) 8–10, https://doi.org/10.1590/s1517-707620170002.0173.
[47] M. Cai, H. Takagi, A.N. Nakagaito, Y. Li, G.I.N. Waterhouse, Effect of alkali treatment on interfacial bonding in abaca fiber-reinforced composites, Composer Part A Appl. Sci. Manuf. 90 (2016) 589–597, https://doi.org/10.1016/j.compositesa.2016.08.025.
[48] A.R. Sena Neto, M.A.M. Araujo, F.V.D. Souza, L.H.C. Mattoso, J.M. Marconcini, Characterization and comparative evaluation of thermal, structural, chemical, mechanical and morphological properties of six pineapple leaf fiber varieties for use in composites, Ind. Crop. Prod. 43 (2013) 529–537, https://doi.org/10.1016/j.indcrop.2012.08.001.
[49] S.A. Hosseini, N. Pan, F. Ko, Dynamic mechanical relaxations of electrospun poly (acrylonitrile-co-methyl acrylate) nanofibrous yarn, Textil. Res. J. 87 (2017) 2193–2203, https://doi.org/10.1177/0040517516665265.
[50] S. Spinella, G. Lo Re, J. Bo Liu, J. Dorgan, Polylactide/cellulose nanocrystal nanocomposites: efficient routes for nanofiber modification and effects of nanofiber chemistry on PLA reinforcement, Int. J. Refrig. 43 (2014) 36–49, https://doi.org/10.1016/j.polymer.2015.02.048.This.
[51] N.P. Lorandi, M. Odila, H. Cioffi ++, H. + Ornaghi, Dynamic mechanical analysis (DMA) of polymeric composite materials, Sci. Cum Ind. (Sci. Cum Ind.). 4 (2016) 48–60.
[52] F. Rezaei, R. Yunus, N.A. Ibrahim, Effect of fiber length on thermomechanical properties of short carbon fiber reinforced polypropylene composites, Mater. Des. 30 (2009) 260–263, https://doi.org/10.1016/j.matdes.2008.05.005.
[53] C. Borsoi, L.C. Scienza, A.J. Zattera, Characterization of composites based on recycled expanded polystyrene reinforced with curaua fibers, J. Appl. Polym. Sci. 128 (2013) 653–659, https://doi.org/10.1002/app.38236.